Nanoporous carbide-derived carbon with tunable pore size

YURY GOGOTSI*[1], ALEXEI NIKITIN[1], HAIHUI YE[1], WEI ZHOU[2], JOHN E. FISCHER[2], BO YI[3], HENRY C. FOLEY[3] AND MICHEL W. BARSOUM[1]

[1]Department of Materials Science and Engineering, Drexel University, 3141 Chestnut Street, Philadelphia, Pennsylvania 19104, USA
[2]Department of Materials Science and Engineering, University of Pennsylvania, 3231 Walnut Street, Philadelphia, Pennsylvania 19104-6272, USA
[3]Department of Chemical Engineering, The Pennsylvania State University, University Park, Pennsylvania 16801, USA
*e-mail: gogotsi@drexel.edu

Published online: 3 August 2003; doi:10.1038/nmat957

Porous solids are of great technological importance due to their ability to interact with gases and liquids not only at the surface, but throughout their bulk[1]. Although large pores can be produced and well controlled in a variety of materials[2], nanopores in the range of 2 nm and below (micropores, according to IUPAC classification) are usually achieved only in carbons or zeolites. To date, major efforts in the field of porous materials have been directed towards control of the size, shape and uniformity of the pores. Here we demonstrate that porosity of carbide-derived carbons (CDCs)[3–9] can be tuned with subångström accuracy in a wide range by controlling the chlorination temperature. CDC produced from Ti_3SiC_2 has a narrower pore-size distribution than single-wall carbon nanotubes or activated carbons; its pore-size distribution is comparable to that of zeolites. CDCs are produced at temperatures from 200–1,200 °C as a powder, a coating, a membrane or parts with near-final shapes, with or without mesopores. They can find applications in molecular sieves, gas storage, catalysts, adsorbents, battery electrodes, supercapacitors, water/air filters and medical devices.

Highly crystallized zeolites have a narrow pore-size distribution, but discrete pore sizes and the fine-tuning of pore size are impossible because the pores of zeolites are controlled by a lattice structure. Porous carbons produced by thermal decomposition of organic materials may have pore diameters[10,11] down to 0.3 nm, or mesopores of several nanometres, but they typically have a broad pore-size distribution[12], which limits their ability to separate molecules of different sizes.

To the best of our knowledge, materials with a tunable pore structure at the atomic level and a narrow pore-size distribution do not exist. It has been shown that selective etching of carbides is an attractive technique for the synthesis of various carbon structures from nanotubes[13] to diamonds[14]. Carbon produced by the extraction of metals from carbides[3,4] is called carbide-derived carbon (CDC). Because the rigid metal carbide lattice is used as a template and the metal is extracted layer-by-layer, atomic-level control can be achieved in the synthesis process and the carbon structure can be templated by the carbide structure. Further structure modification and control can be achieved by varying the temperature, gas composition, and other process variables. The reaction:

$$SiC + 2Cl_2(g) = SiCl_4(g) + C \qquad (1)$$

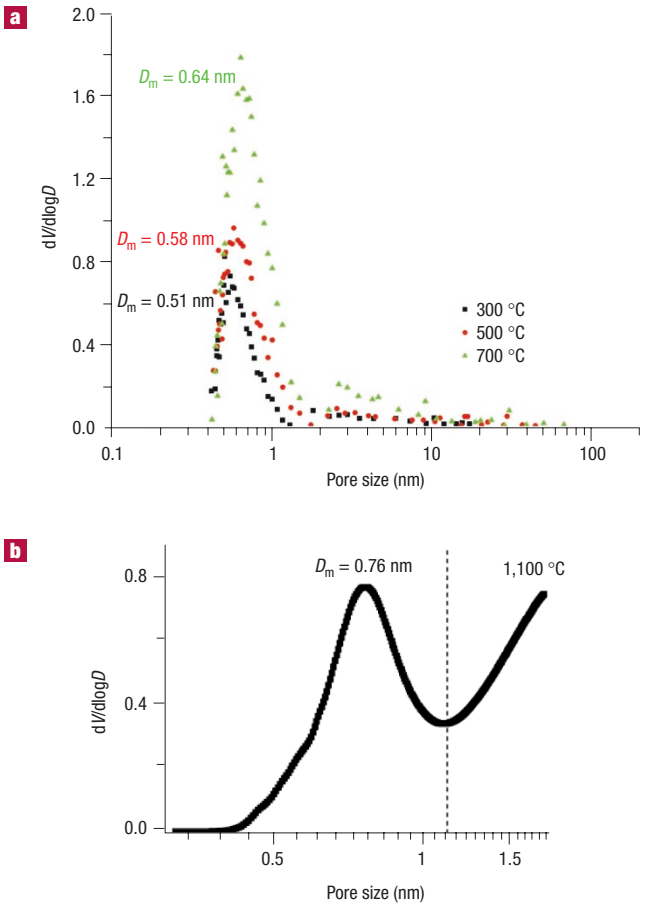

Figure 1 Differential pore-size distributions for CDC. a, Measured by methyl chloride and **b**, measured by argon adsorption technique. No mesopores or macropores were detected at 300–500 °C. A small volume of mesopores of 2–4 nm in size appears at 700 °C, and the volume of mesopores increases sharply at 1,100 °C and above. Distributions were calculated using the Horvath–Kawazoe method and assuming a slit-pore model. Ar adsorption was measured at –186 °C. D_m is the pore size corresponding to the maximum in pore-size distribution.

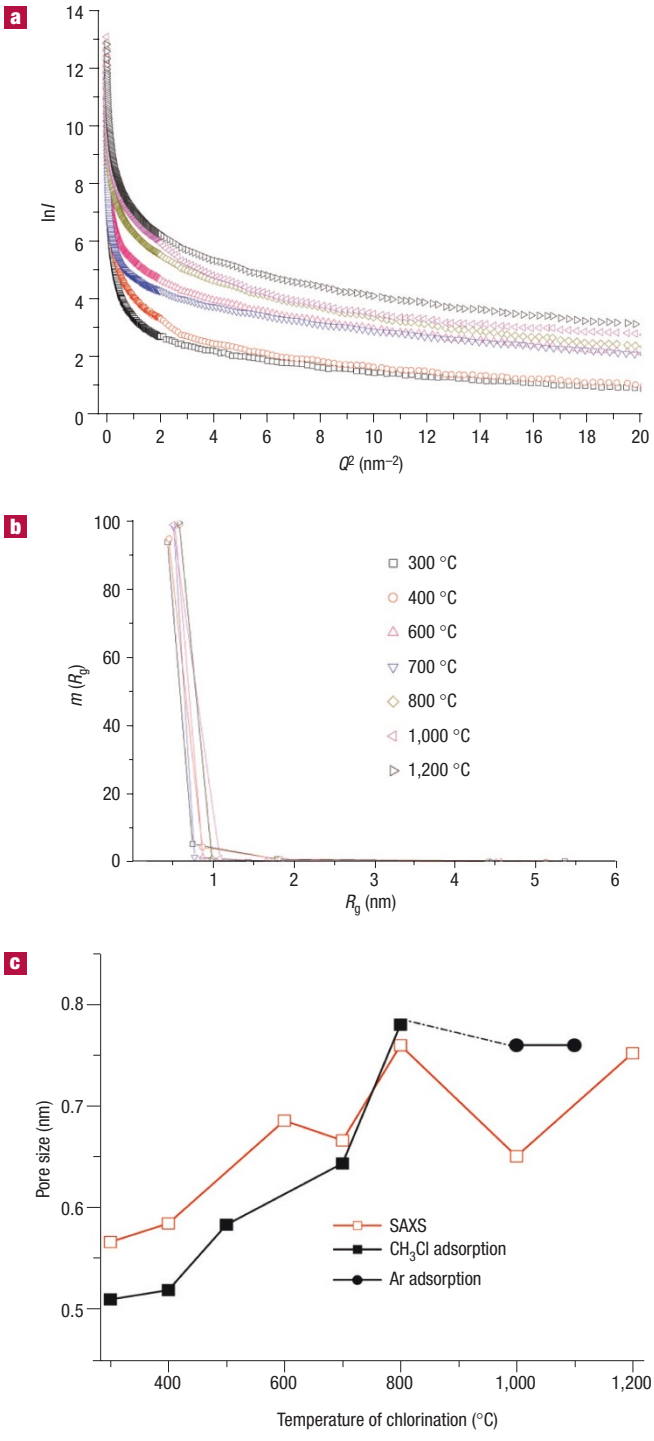

Figure 2 Dependences of the radius of gyration (R_g) and pore size on chlorination temperature. a, Experimental small-angle X-ray scattering (SAXS) curves in Guinier coordinates. **b**, Distribution of gyration radius $m(R_g)$. **c**, Comparison of pore sizes obtained by CH_3Cl sorption and SAXS for different chlorination temperatures of Ti_3SiC_2. No pores with R_g larger than 0.6 nm were detected by SAXS. The SAXS-derived R_g at 600 °C is 0.53 nm, and the sorption-based D_m (average of 500 °C and 700 °C values) is 0.61 nm. Taking the latter as the height of slit pores, the implied radius R is 0.71 nm, comparable to the radii of slit-shaped nanopores in polymer-derived materials[12]. Thus, slit pores have been formed in CDC. Extremely fine tuning of pore sizes is possible between 300 °C and 800 °C. At higher temperatures, growth of mesopore volume occurs at the expense of nanopores.

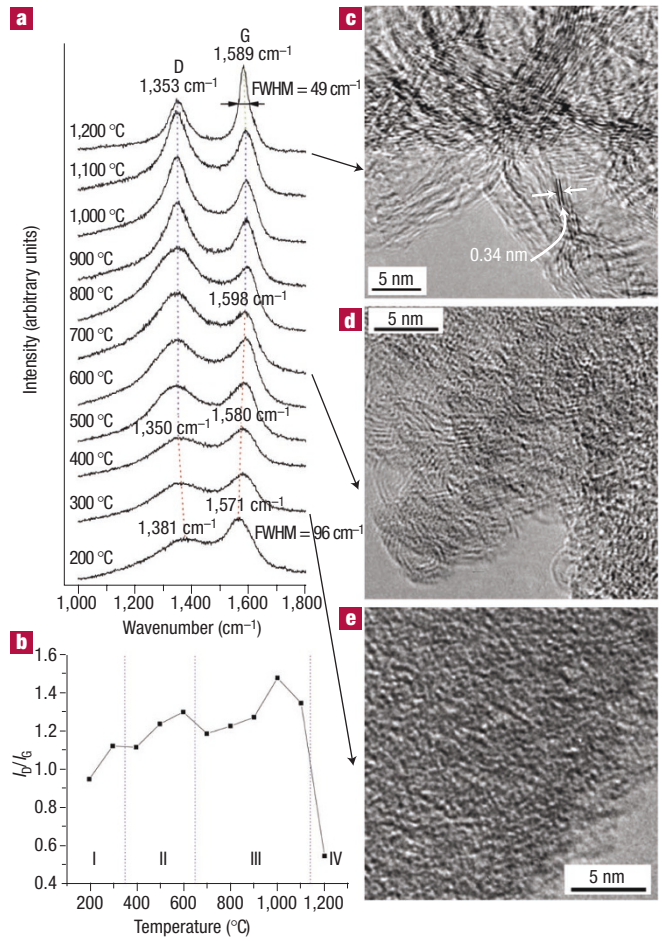

Figure 3 Raman spectra and transmission electron microscope (TEM) images of CDC produced at different temperatures. a, Raman spectra of CDC synthesized at different temperatures. **b**, The temperature dependence of the ratio of the intensities of disorder-induced D band and graphite G band (I_D/I_G). **c–e**, TEM images showing evolution of the carbon structure with temperature: **c**, 1,200 °C, **d**, 700 °C, **e**, 300 °C. CDC produced in temperature range I (300 °C; see part **b**) is completely amorphous. Slow pore growth occurs in range II. Formation of carbon fringes at 700 °C and higher temperatures shows the beginning of the structure ordering leading to increasing pore size and appearance of mesopores in range III. Pronounced graphitization is observed at 1,200 °C (range IV), resulting in a sharper G-band in the Raman spectrum and decreased I_d/I_g ratio.

has been used for the production of silicon tetrachloride since 1918[6], but the remaining carbon was usually burned. The linear reaction kinetics of the reaction (1)[5] allows transformations to large depth, until the particle or component is completely converted to carbon. The transformation is conformal and does not lead to changes in sample size or shape.

Various CDCs have been investigated by several groups and specific surface areas (SSA) of up to 2,000 $m^2\,g^{-1}$ with small pore sizes have been reported[4,7–9]. Comparison of literature data on CDCs shows that, for different carbides (SiC, TiC, ZrC, B_4C, TaC and Mo_2C) and chlorination temperatures, pores between 0.8 and 2.1 nm, determined by the structure of the carbide precursor and process parameters, were produced. However, no control over the pore size or distribution has been reported. The objective of this work is to demonstrate pore-size tuning in CDCs by controlling the synthesis temperature.

This study was conducted on Ti_3SiC_2 powders and bulk samples. Ti_3SiC_2 is a soft ceramic with a lamellar structure (Supplementary Information, Fig. S1) that is commercially available and can easily be machined to any shape[15]. Etching of Ti_3SiC_2 can generate a larger pore volume (~75%) compared with TiC or SiC (56.2% and 57.3%, respectively; Supplementary Information, Table S1). Its interaction with chlorine, Cl_2, has not been reported in the literature.

Chlorination in a flow of pure Cl_2 for 3 hours in a quartz-tube furnace results in extraction of Ti and Si from Ti_3SiC_2 leading to the formation of carbon by the reaction:

$$Ti_3SiC_2 + 8Cl_2(g) = SiCl_4(g) + 3TiCl_4(g) + 2C \qquad (2)$$

Four different techniques were independently used to measure the pore size: Ar, N_2 and methyl chloride (CH_3Cl) sorption, as well as small-angle X-ray scattering (SAXS), as described in the Methods. As can be seen in Fig. 1, pore sizes of CDCs increase with increasing temperature. The sorption isotherms of low-temperature CDCs (up to 600 °C) obtained using N_2, Ar, or, CH_3Cl (Supplementary Information, Fig. S2), were of type I in the Brunauer classification[12], which is evidence of the presence of nanopores and the absence of meso- or macropores. This is in agreement with the differential pore-size distributions shown in Fig. 1a. Very small pore sizes were achieved at low temperatures; just slightly larger than the interplanar spacing in graphite (0.3354 nm). What is even more impressive is the fact that the pore-size distributions are very narrow (Fig. 1a) and close to those of, for example, VPI-5 zeolite[1].

Isotherms of CDCs produced above 700 °C were of type IV, which indicates the presence of mesopores. Total pore volumes observed for the samples produced at 700, 900 and 1,100 °C were almost the same, but the pore-size distributions were different: mesopore volume and size increased with increasing chlorination temperatures. Their equivalent radius was less than 3 nm at 700 °C (Fig. 1a) and about 6 nm at 1,100 °C (Fig. 1b). Weight loss and energy-dispersive X-ray spectroscopy (EDS) analysis of the samples after chlorination suggested almost complete removal of Ti and Si above 400 °C. Because the CDCs retained the original volume of the carbide precursor, it is fair to assume the total pore volume to be the same after chlorination at different temperatures. The maximum pore volume of ~0.64 $cm^3\ g^{-1}$ accessible to Ar and N_2 in CDC after heat-treatment at 700–1,200 °C is in agreement with the theoretically calculated value of 0.645 $cm^3\ g^{-1}$.

SAXS measurements confirm the evolution of pore size with increasing processing temperature. In Fig. 2, we plot the data for seven samples spanning the range between 300 °C and 1,200 °C. The results have been corrected for background and scattering by the quartz container. We observe almost monodisperse Guinier behaviour, $\log(I) \sim -Q^2(R_g)^2/3$ over a broad range of Q^2 (Fig. 2a), where I is the intensity, and R_g is the radius of gyration, as shown by the fact that the analysis using a technique described elsewhere[16] gives a very narrow peak in $m(R_g)$ which accounts for most of the nanopore volume (Fig. 2b). The interpretation of R_g (Fig. 2c) depends on the shape of the nanopores. In the analysis of the CH_3Cl sorption data we assumed slit pores, which implies that the sizes in Fig. 1 are associated with the height of the slits. Slit pores are the logical choice, given the layered nature of the precursor material (Supplementary Information, Fig. S1). For slit pores approximated as cylinders of radius R and height D, $R_g^2 = D^2/12 + R^2/2$. SAXS confirms the aforementioned sorption data and shows that pore size can be controlled with better than 0.05 nm accuracy (Fig. 2c), which, to our knowledge, has never been demonstrated for any other porous material.

A kinetic model of self-organization in the formation of nanopores during chlorination of SiC has been proposed[8]. It can be used to describe the formation of the ordered nanoporous carbon from Ti_3SiC_2. With increasing temperature, the specific jump distance of carbon atoms increases and the pore size increases accordingly.

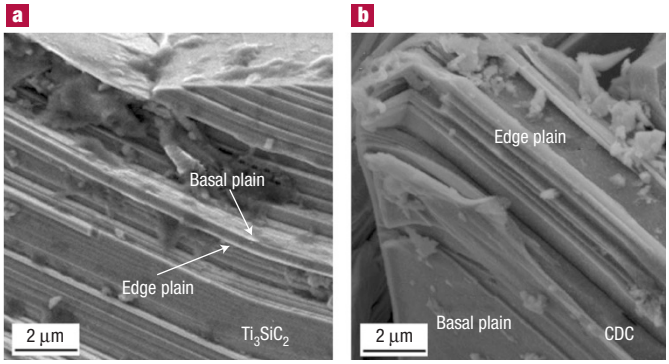

Figure 4 Scanning electron microscope images of a sample surface. a, The as-received sample. **b**, After chlorination at 300 °C. The lamellar structure of Ti_3SiC_2 is clearly seen. **b**, Fully amorphous carbon, which maintains the lamellar structure of the carbide.

Microstructural studies of CDCs were conducted to explain their structural reorganization and the development of their porous structure with temperature. Raman spectroscopy (Fig. 3a,b) shows that carbon already forms at 200 °C. However, X-ray diffraction (XRD) shows peaks of the initial carbide; thus the transformation was not complete at this temperature. A low position of the G-band and upshifted D-band in the Raman spectrum (Fig. 3a) may be the result of carbon bonding to Si and significant sp^3 hybridization of carbon[17]. Si (<15%) was detected by EDS in the samples chlorinated at 300 °C, showing that Ti was preferentially etched at lower temperatures. Different rates of Si and Ti reaction were also observed[18] in carburization and silicidation of Ti_3SiC_2 above 1,400 °C. Experiments on TiC (Ref. 19) and SiC (Ref. 20) show that Ti can be extracted by Cl_2 at lower temperatures than Si. Complete removal of Si from CDC and a decreased amount of trapped chlorine (Supplementary Information, Fig. S3) leads to an increase in pore volume from 0.25 $cm^3\ g^{-1}$ at 300 °C to 0.645 $cm^3\ g^{-1}$ at 700 °C. A slow increase in intensity and downshift of the D band in the Raman spectra are observed with increasing temperature. According to high-resolution transmission electron microscopy (TEM) analysis and selected-area diffraction, the CDC samples produced at lower temperatures were completely amorphous (Fig. 3e). Noticeable ordering of graphite starts at 700 °C (Fig. 3d) and nanocrystalline graphite appears at 1,200 °C (Fig. 3c). The full-width at half-maximum (FWHM) of the G-band decreases slightly above 600 °C, but only at 1,200 °C does Raman spectroscopy show the formation of ordered graphitic carbon. Very thin (2–5 graphene layers) sheets of graphite are clearly seen in TEM (Fig. 3c).

Total volume and characteristic dimensions of meso- and nanopores can be controlled by selection of a binary or ternary carbide or a carbide solid solution and variation of the chlorination process parameters. For example, carbon derived from SiC at 900 °C has a narrow pore-size distribution and an average pore size of 0.65 nm, similar to CDCs produced from Ti_3SiC_2 at 700 °C, but with no mesopores. Carbon made from SiC at 1,200 °C had a pore size of 1.2 nm, and values from 0.8 to 2.1 nm were reported in literature for SiC- and B_4C-derived carbons[21]. Depending on the carbide structure (Supplementary Information, Table S1), the pore volume of CDCs can vary from ~50% to ~80%. CDCs derived from Ti_3SiC_2 have the theoretical density of 0.55 g cm^{-3}. CDC samples are hydrophilic and adsorb water quickly; rapidly sinking in water. However, if the surface is sealed with nail polish, they float because their density is well below 1 g cm^{-3}.

It is notable that CDCs do not have macroporosity if produced from a dense ceramic (Fig. 4) or a carbide single crystal. However, a controlled amount of macroporosity can be introduced by using sintered porous ceramics. Macroporosity or mesoporosity that appear at high chlorination temperatures is not desirable for molecular-sieve membranes, but would be necessary for catalytic and some other applications, because it allows easier access to nanopores.

Based on their tunable porous structures, controlled surface chemistry, and other properties, CDCs may be used for some applications where single-wall carbon nanotubes are currently considered[22]. For example, CDC is an attractive material for electrodes for electrochemical double-layer capacitors commonly called 'supercapacitors'[23], because the pore-size distribution can be tuned to match various electrolytes.

Finally, it is known that hydrogen uptake depends on the porous structure of the adsorbent. The highest uptake was achieved in nanoporous carbons with SSA above 1,000 $m^2\ g^{-1}$ and almost no mesopores[24,25]. CDCs produced at 600 °C and 1,100 °C have SSA of 1,061 $m^2\ g^{-1}$ and 1,431 $m^2\ g^{-1}$, respectively, and SSA of up to 2,000 $m^2\ g^{-1}$ has been measured for SiC- and B_4C-derived CDC. Our ability to tune the pore size to exactly fit the hydrogen (or other gas) molecule may be of principal importance for gas storage applications. About 40 wt% Cl_2 is trapped in CDCs produced at 300–400 °C at room temperature and ambient pressure, if the cooling is done in argon, and it can reach 55–60 wt% when cooled in Cl_2. The amount of Cl_2 stored decreases with increasing pore size, reaching less than 5 wt% at 1,200 °C (Supplementary Information, Fig. S3). The stored chlorine is slowly released, and its amount goes down to ~20 wt% after storage for ten days in open air. Fast release of atomic chlorine is observed on heating in helium up to 600 °C at 10 °C min^{-1}. Attempts to measure SSA of CDC produced at 300 °C by the BET method resulted in the unreasonably low values of 162 $m^2\ g^{-1}$ for N_2 and 382 $m^2\ g^{-1}$ for Ar. This clearly shows the selectivity of CDC to different gases. A significant volume of nanopores inaccessible to large molecules may allow for the separation of hydrogen from N_2 and other gases. It is also worth noting that the combination of near-final shape and very mild chlorination temperatures are not only unique to Ti_3SiC_2, but also bode well for the inexpensive mass production of CDC components, which, unlike zeolites, can have a large size and complex shape.

METHODS

The total pore volume and average pore size were calculated from Ar and CH_3Cl adsorption isotherms according to Horvath–Kawazoe theory. Specific surface area—according to BET (Brunauer, Emmet and Teller) theory and nanopore volume—was calculated by using t-plots based on the CH_3Cl or Ar sorption isotherms. Nitrogen adsorption did not produce reliable results on samples with a pore size smaller than 1 nm. Ar adsorption (Micromeretics ASAP Pore Analyzer) was used to measure pore sizes above and under 1 nm, but the technique required long periods of time (5 days) for equilibration and could not produce the full distribution when the pore size approached 0.5 nm. The methyl chloride adsorption isotherms[26] were used to measure the pore size below 0.7 nm assuming a slit pore shape.

Small-angle X-ray scattering (SAXS) was performed on a multi-angle diffractometer equipped with a Cu rotating anode, double-focusing optics, evacuated flight path and two-dimensional wire detector. Data were collected over the Q range 0.005–1.4 $Å^{-1}$. Powder samples were loaded into 1.5-mm-diameter quartz capillary tubes and measured in transmission for 1 hour. The scattering intensity from an empty capillary was then collected and subtracted with sample absorption corrected. Expecting a finite but narrow distribution of radii of gyration R_g, we used a modified Guinier analysis to obtain the mean pore size and distribution[16]. The fraction volume of pores of a given size was then estimated for each sample. By deconvoluting the experimental $\ln(I)$ versus Q^2 curves into components corresponding to pores with different R_g, distribution functions of R_g were found.

Raman microspectroscopy (Renishaw 1000, Ar ion laser, 514.5 nm), transmission electron microscopy (TEM, JEOL 2010F), energy-dispersive spectroscopy (EDS) and X-ray diffraction (XRD, Siemens), were used to study the structure of CDC powders. The in-plane crystal size of graphite L_a (nm) was calculated by the Tuinstra and Koenig equation[27]: $0.44/L_a = I_D/I_G$, where I_D and I_G are intensities of disorder-induced D band and graphite G band, assigned to zone centre phonons of E_{2g} symmetry[17].

Received 11 March 2003; accepted 10 July 2003; published 3 August 2003.

References

1. Davis, M. E. Ordered porous materials for emerging applications. *Nature* **417,** 813–821 (2002).
2. Joo, S. H. *et al.* Ordered nanoporous arrays of carbon supporting high dispersions of platinum nanoparticles. *Nature* **412,** 169–172 (2001).
3. Gogotsi, Y. G. & Yoshimura, M. Formation of carbon films on carbides under hydrothermal conditions. *Nature* **367,** 628–630 (1994).
4. Gogotsi, Y. G., Jeon, J. D. & McNallan, M. J. Carbon coatings on silicon carbide by reaction with chlorine-containing gases. *J. Mater. Chem.* **7,** 1841–1848 (1997).
5. Ersoy, D., McNallan, M. J. & Gogotsi, Y. G. Carbon coatings produced by high temperature chlorination of silicon carbide ceramics. *Mater. Res. Innov.* **5,** 55–62 (2001).
6. Hutchins, O. Method for the production of silicon tetrachlorid. US patent 1,271,713 (1918).
7. Boehm, H. P. & Warnecke, H. H. in *Proc. 12th Biennial Conf. Carbon* 149–150 (Pergamon, Oxford, 1975).
8. Gordeev, S. K., Kukushkin, S. A., Osipov, A. V. & Pavlov, Y. V. Self-organization in the formation of a nanoporous carbon material. *Phys. Solid State* **42,** 2314–2317 (2000).
9. Fedorov, N. F. Untraditional solutions in chemical technology of carbon adsorbents. *Russ. Chem. J.* **39,** 73–83 (1995).
10. Claye, A. & Fischer, J. E. Short-range order in disordered carbons: where does the Li go? *Electrochim. Acta* **45,** 107–120 (1999).
11. Shiflett, M. B. & Foley, H. C. Ultrasonic deposition of high-selectivity nanoporous carbon membranes. *Science* **285,** 1902–1905 (1999).
12. Rodriguez-Reinoso, F. & Sepulveda-Escribano, A. in *Handbook of Surfaces and Interfaces of Materials* (ed. Nalwa, H. S.) 309–355 (Academic, San Diego, 2001).
13. Derycke, V., Martel, R., Radosavljević, M., Ross, F. M. & Avouris, P. Catalyst-free growth of ordered single-walled carbon nanotube networks. *Nano Lett.* **2,** 1043–1046 (2002).
14. Gogotsi, Y., Welz, S., Ersoy, D. A. & McNallan, M. J. Conversion of silicon carbide to crystalline diamond-structured carbon at ambient pressure. *Nature* **411,** 283–287 (2001).
15. Barsoum, M. W. The $M_{n+1}AX_n$ phases: a new class of solids. *Prog. Solid State Chem* **28,** 201–281 (2000).
16. Kyutt, R. N., Smorgonskaya, E. A., Danishevski, A. M., Gordeev, S. K. & Grechinskaya, A. V. Structural study of nanoporous carbon produced from polycrystalline carbide materials: small-angle X-ray scattering. *Phys. Solid State* **41,** 1359–1363 (1999).
17. Ferrari, A. C. & Robertson, J. Interpretation of Raman spectra of disordered and amorphous carbon. *Phys. Rev. B* **61,** 14095–14107 (2000).
18. El-Raghy, T. & Barsoum, M. W. Diffusion kinetics of the carburization and silicidation of Ti_3SiC_2. *J. Appl. Phys.* **83,** 112–119 (1998).
19. Leis, J., Perkson, A., Arulepp, M., Nigu, P. & Svensson, G. Catalytic effect of metals of the iron subgroup on the chlorination of titanium carbide to form nanostructural carbon. *Carbon* **40,** 1559–1564 (2002).
20. Gogotsi, Y. *et al.* Formation of carbon coatings on SiC fibers by selective etching in halogens and supercritical water. *Ceram. Eng. Sci. Proc.* **19,** 87–94 (1998).
21. Yanul', N. A. *et al.* Nanoporous carbon materials with varied porosity and specific features of their interaction with water. *Russ. J. Appl. Chem.* **72,** 2159–2163 (1999).
22. Baughman, R. H., Zakhidov, A. A. & de Heer, W. A. Carbon nanotubes - the route toward applications. *Science* **297,** 787–792 (2002).
23. Burke, A. Ultracapacitors: why, how, and where is the technology? *J. Power Sources* **91,** 37–50 (2000).
24. Nijkamp, M. G., Raaymakers, J. E. M. J., van Dillen, A. J. & de Jong, K. P. Hydrogen storage using physisorbtion — materials demands. *Appl. Phys. A.* **72,** 619–623 (2001).
25. Schlapbach, L. & Züttel, A. Hydrogen-storage materials for mobile applications. *Nature* **414,** 353–358 (2001).
26. Mariwala, R. K. & Foley, H. C. Calculation of micropore sizes in carbogenic materials from the methyl chloride adsorption isotherm. *Ind. Eng. Chem. Res.* **33,** 2314–2321 (1994).
27. Tuinstra, F. & Koenig, J. L. Raman spectrum of graphite. *J. Chem. Phys.* **53,** 1126–1130 (1970).

Acknowledgements

Thanks are due to W.-H. Shih, Drexel University, for help with nitrogen BET measurements. The work at Drexel University was supported by the Defence Advanced Research Projects Agency through an Office of Naval Research (ONR) contract. The TEM used is operated by the Regional Materials Characterization Facility at the University of Pennsylvania. Purchase of the Raman spectrometer and SEM were supported by National Science Foundation (NSF) grants DMR-0116645 and BES-0216343. The work at Pennsylvania State University was supported by ONR grant N00014-00-1-0720 and NSF grant DMR-0103585. M.B. was supported by NSF grant DMR-0072067.

Correspondence and requests for materials should be addressed to Y.G.

Supplementary Information accompanies the paper on http://www.nature.com/naturematerials

Competing financial interests

The authors declare that they have no competing financial interests.